Effects of fuel-capsule shimming and drive asymmetry on inertial-confinement-fusion symmetry and yield

F. H. Séguin,[1] C. K. Li,[1] J. L. DeCiantis,[1,a)] J. A. Frenje,[1] J. R. Rygg,[1,b)] R. D. Petrasso,[1] F. J. Marshall,[2] V. Smalyuk,[2,b)] V. Yu. Glebov,[2] J. P. Knauer,[2] T. C. Sangster,[2] J. D. Kilkenny,[3] and A. Nikroo[3,b)]
[1]*Plasma Science and Fusion Center, Massachusetts Institute of Technology, Cambridge, Massachusetts 02139, USA*
[2]*Laboratory for Laser Energetics, University of Rochester, Rochester, New York 14623, USA*
[3]*General Atomics, San Diego, California 92121, USA*

(Received 12 October 2015; accepted 29 February 2016; published online 22 March 2016)

Three orthogonal proton emission imaging cameras were used to study the 3D effects of low-mode drive asymmetries and target asymmetries on nuclear burn symmetry and yield in direct-drive, inertial-confinement-fusion experiments. The fusion yield decreased quickly as the burn region became asymmetric due to either drive or capsule asymmetry. Measurements and analytic scaling are used to predict how intentionally asymmetric capsule shells could improve performance by compensating for drive asymmetry when it cannot be avoided (such as with indirect drive or with polar direct drive). © *2016 AIP Publishing LLC*. [http://dx.doi.org/10.1063/1.4943883]

I. INTRODUCTION

The object of inertial-confinement fusion (ICF) is to compress a fuel capsule to a state with high enough density and temperature to ignite, starting a self-sustaining fusion burn that consumes much of the fuel and releases a large amount of energy.[1,2] Compression is accomplished by driving the capsule with radiation, usually in the form of either laser light (direct drive) or x rays generated by laser light striking the inner walls of a small chamber, or hohlraum, containing the capsule (indirect drive). Ignition will be sparked by the products of nuclear fusion reactions in the hot, compressed core. Efficient conversion of drive energy to fusion energy requires that the fuel be assembled into a symmetric configuration, and achievement of ignition is expected to require that any low-mode asymmetry of the burning fuel be on the level of 2% or less.[1] Two problems that can prevent symmetric fuel compression, and greatly reduce the yield of the initial fusion burn that will spark ignition, are asymmetry in the drive or asymmetry in the capsule.

In direct-drive experiments such as those normally performed at the OMEGA Laser System,[3] both the fuel capsule and the laser drive are symmetric by design. In some other scenarios, true symmetric drive is difficult to achieve. With indirect drive, which is the standard approach at the National Ignition Facility (NIF),[1] x-ray illumination on the capsule is axially symmetric but not quite spherically symmetric because of the cylindrical geometry of the hohlraum. (Methods that have been proposed or implemented for minimizing drive asymmetry in hohlraums have included use of "shine shields" inside the laser-entrance holes,[4] adjustments in the positions where lasers illuminate the inside wall of the hohlraum,[5] and use of different laser wavelengths for different laser beams.[6])

A version of direct drive at the NIF utilizes laser beams positioned as for indirect drive, with axial symmetry but predominately from the polar directions. The approach for this "Polar Direct Drive"[7,8] is to repoint the beams slightly and vary their intensities to come as close as possible to spherical symmetry, but there will always be more drive at the poles than at the equator.

For these situations in which some drive asymmetry is unavoidable, it has been suggested[7,9] that capsule shells intentionally asymmetric in thickness ("shimmed") might improve implosion symmetry. Here, we present new and quantitative experimental observations (e.g., Fig. 1) demonstrating that in direct-drive ICF experiments both drive asymmetry and capsule-shell asymmetry have predictable effects on three-dimensional asymmetries in the spatial distribution of nuclear burn, indicating that capsule shimming could be used to control implosion asymmetry in a predictable way. This has just been experimentally tested in the polar-direct-drive context at OMEGA,[10] and it will soon be tested in indirect-drive experiments at the NIF.[11]

The experimental results were shown to be approximately consistent with a simple scaling law that equalizes radial implosion velocity at different angles through acceleration and coasting phases by balancing the local force of ablation with the local shell thickness. The result is a quantitative prediction of how shimming could be used to counteract some of the negative effects of low-mode drive asymmetry.

II. EXPERIMENTS

A. Procedure

Observations of direct-drive implosions at OMEGA were made using three orthogonal proton emission imaging

[a)]Present address: AREVA, Inc., Lynchburg, Virginia 24503, USA.
[b)]Present address: Lawrence Livermore National Laboratory, Livermore, California 94550, USA.

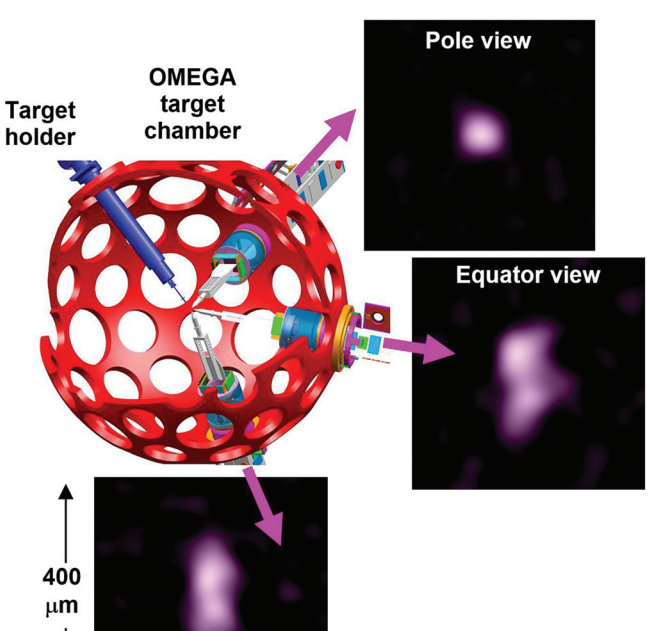

FIG. 1. Three proton-emission images recorded from orthogonal directions show how asymmetric D^3He burn results from (intentional) drive asymmetry in experiments at OMEGA (lighter color means more D^3He reactions). The target capsule was spherical (Fig. 2(b)). Laser intensity was axially symmetric, and lower than average in the pole directions (Fig. 2(a), curve $(A_2/A_0) = -0.36$ resulting in an elongated, or prolate, burn distribution.

cameras[12–14] to study the spatial distribution of D^3He fusion burn by recording 14.7-MeV D^3He protons. To the best of our knowledge, the images in Fig. 1 were the first burn images made with D^3He protons and the first complete set of three orthogonal burn images of any kind. (DT burn regions have been studied with neutron imaging from one direction,[15–18] and just recently our approach was used to look at the D^3He burn region in a Polar Direct Drive implosion at the NIF.[19]) Each imaging camera utilized a penumbral aperture, a CR-39 imaging detector, and a spatial deconvolution algorithm described previously[12,20] to provide a two-dimensional image of the three-dimensional distribution of fusion reactions and to provide an absolute measurement of the total D^3He yield.

The nuclear burn images, which integrate over the total burn interval of ~150 ps, are of fundamental importance because they reflect the cumulative effects on the fuel of drive and all of the physics affecting implosion dynamics. To complement the burn images, x-ray emission images[21,22] filtered to be sensitive mostly to shell emission were also recorded to provide a more complete picture and a consistency check. In each experiment, x-ray framing cameras viewed the plasma from directions opposite two of the burn-imaging cameras.

The experiments involved the use of laser drive with angular variations in on-target intensity or capsules with angular variations in shell thickness. Spatial distributions of drive, capsule shell thickness, and burn are each represented here as sums of Legendre polynomials $\sum_\ell A_\ell P_\ell(\cos\theta)$. We are interested here in low mode numbers and will refer

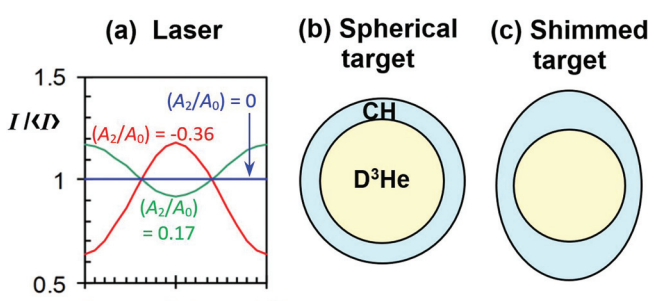

FIG. 2. Three angular distributions of laser intensity I on target (a), and structures of spherical (b) and shimmed (c) targets. Each intensity distribution is labeled with the ratio of its 2nd and 0th Legendre amplitudes.

primarily to P_2 asymmetries that are quantified by the ratio A_2/A_0.

B. Effects of drive asymmetry

The effects of drive asymmetry on spherical capsules were studied using 17-μm-thick CH shells with 860-μm outer diameters, filled with 20 atm of D^3He gas (Fig. 2(b)). Laser drive was provided by 60 OMEGA beams in a 1-ns-square, 18-kJ pulse, but the intensities of individual beams were adjusted to produce nearly pure P_2 distortions with several values of the ratio $(A_2/A_0)_{drive}$ spanning the range from -0.36 to $+0.17$, as illustrated in Fig. 2(a). The images in Fig. 1, recorded from along the drive symmetry axis (at the "pole") and from two nearly orthogonal directions (on the "equator") for $(A_2/A_0)_{drive} = -0.36$, show that the burn region was prolate, elongated in the direction of the axis of drive symmetry. This was expected, since the equator was driven hardest.

Contour plots of Fig. 1 images are shown in Fig. 3(a), along with contour plots for two other cases. In the symmetric-drive case $(A_2/A_0)_{drive} = 0$, the pole and equator images are both fairly round and equal in size, indicating a spherically symmetric burn. In the case $(A_2/A_0)_{drive} = 0.17$, the pole view is fairly round (but larger than the symmetric-drive case) while the equator view is somewhat elongated in the direction perpendicular to the polar axis, indicating an oblate burn distribution.

It is useful to compare spatial distributions of nuclear burn to the x-ray emission images of the shell that were recorded at approximately the same time and that are dominated by radiation from the hottest shell material at the fuel-shell interface. For the burn distribution of Fig. 1 (and Fig. 3(a)), the result is shown in Fig. 4, where it can be seen that the main burn-image structures and sizes are compatible with the x-ray-inferred shell structure (see also Fig. 5, below, and Ref. 14 for other comparisons of D^3He burn region size to x-ray images). The brightness of the central portion of the equatorial x-ray image appears to indicate convergence of hot shell material on the symmetry axis, which would explain why the D^3He fusion yield is lower there.

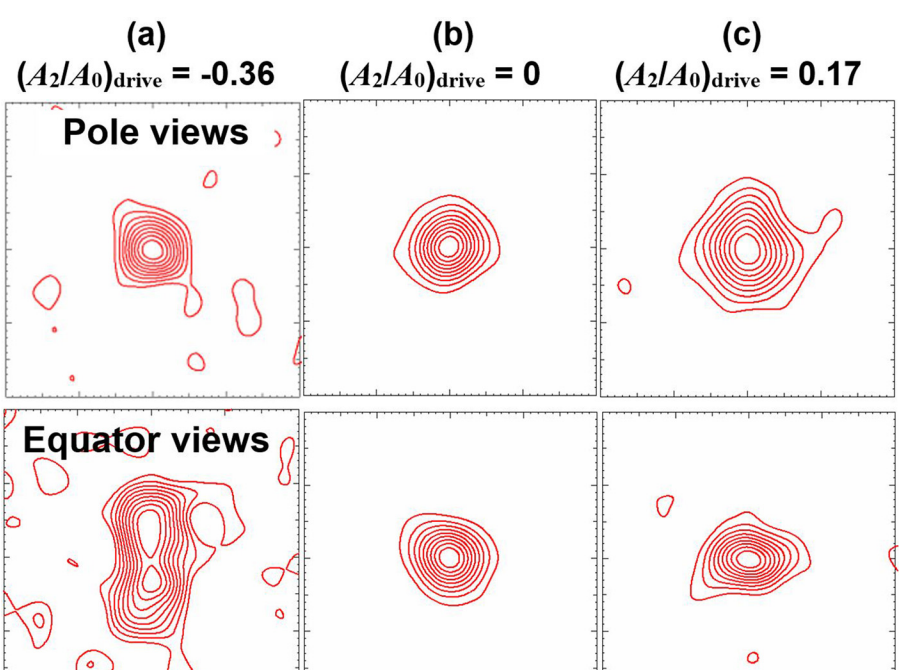

FIG. 3. Contour plots of burn images of spherical capsules show that asymmetries in the burn result in a predictable way from asymmetries in the drive. The contours are linearly spaced at 10%, 20%,…, 90% of the peak value. The data come from (a) OMEGA shots 35 172 and 35 173 (summed), (b) 36 020, and (c) 35 174. As discussed in the Appendix, the statistics-constrained spatial resolutions of these burn distributions are 20 μm for (b) and (c) but 35 μm for (a), because of the very low proton yield for this case. The noise structures outside the main burn region indicate the spatial scale and amplitude of noise-generated spurious structure in the inferred burn distribution.

C. Effects of target capsule shimming

The effects of target shimming were studied in separate experiments using 860-μm-diameter, 20-μm-thick CH shells filled with 18 atm of D^3He, and symmetric drive in a 1-ns-square, 22-kJ pulse. A symmetric (spherical) capsule was imploded for reference, and D^3He burn images indicated spherical symmetry. Shimmed capsules tried next (Fig. 2(c)) were similar, except that the shell thickness was 19.1 μm at the equator and 21 μm at the pole $[(A_2/A_0)_{shell} = 0.07]$. Results for this case are shown in Fig. 5. The nuclear burn images indicate that the spatial distribution of fusion reactions was prolate, with symmetry axis aligned with the shimmed-target axis; there was less compression of the hot fuel where the shell was thicker. In addition, the nuclear burn images correlate well with an x-ray image recorded near peak burn time. As shown in Fig. 5, the x-ray image demonstrates that the inner shell surface was also prolate, with the same axis of symmetry as the burn image and with a slightly larger size.

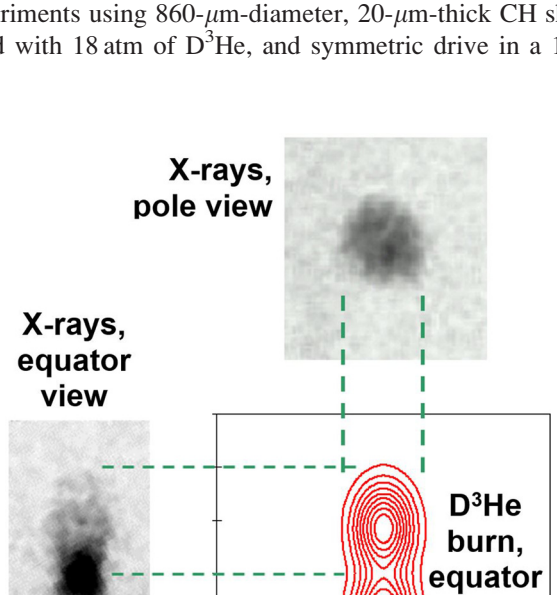

FIG. 4. X-ray emission images of the shell near peak burn time from OMEGA shot 35 173, compared to the inferred distribution of fusion burn from shots 35 172 and 35 173 with drive asymmetry $(A_2/A_0)_{drive} = -0.36$. The x-ray images have a spatial resolution of about 10 μm. The original burn images, shown in Figs. 1 and 3(a), have a resolution of 35 μm (because very low yield required serious filtering) so for comparison the burn distribution shown here is an estimate of the true burn distribution derived as discussed in the Appendix. (This estimation process was not necessary for the burn images shown in Fig. 5, which come from a higher-yield shot.)

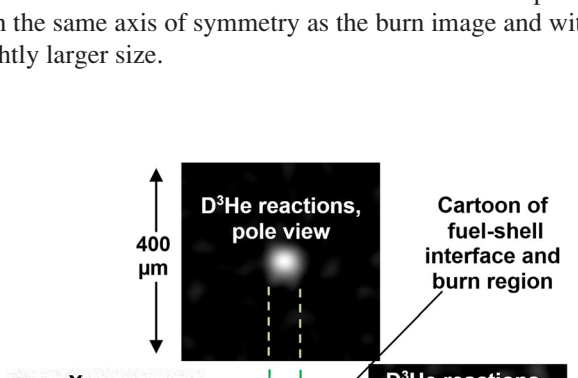

FIG. 5. Images of the spatial distribution of D^3He reactions in the compressed fuel (top and right), and the spatial distribution of 4–5 keV x-rays from the fuel-shell interface (left), at peak burn time for OMEGA shot 40 532 utilizing the shimmed target.

D. Quantitative overview

Quantitative results of all experiments are summarized in Fig. 6, where the top two plots show the asymmetries of the burn regions and the bottom two plots show the D^3He-proton yields and the DD-neutron yields (measured as described in Ref. 23). Although the asymmetric-drive and asymmetric-capsule experiments utilized slightly different capsule shell thicknesses, fill pressures, and drive energies, they were quite similar and allow us to make some general comparisons. From Fig. 6, it can be seen that deviations of either drive or shell thickness from spherical symmetry lead to a rapid falloff of fusion yield in conjunction with a loss of burn symmetry. Furthermore, both drive asymmetry and shell asymmetry lead to burn asymmetry in systematic and expected ways. This implies that it should be possible to compensate for drive asymmetry with an appropriate amount of shell asymmetry. From the slopes of the two upper plots, which differ by a factor of about −2.5, we could predict that an implosion would be approximately symmetric if $(A_2/A_0)_{\text{shell}} \approx 0.4\ (A_2/A_0)_{\text{drive}}$. Keeping in mind the fact that this conclusion is based on slightly mismatched experimental conditions, we will now try to understand it and make more general predictions.

III. DISCUSSION

The burn-asymmetry trends seen in Fig. 6 are logical consequences of the "rocket equations,"[1,2] which describe the development of shell implosion velocity V in response to pressure from the illumination-induced ablation of shell material at rate $\dot{m}$ (g/cm^2/s), with exhaust velocity v_{ex}: $dV/dt = v_{ex}M^{-1}dM/dt$, where M is the shell mass per unit solid angle, $dM/dt = -R^2\dot{m}$, and $R(t)$ is the shell radius. The effects of illumination intensity I are approximately $\dot{m} \cong A\,I^a$ and $v_{ex} \cong B\,I^b$, where A, B, a, and b are constants that

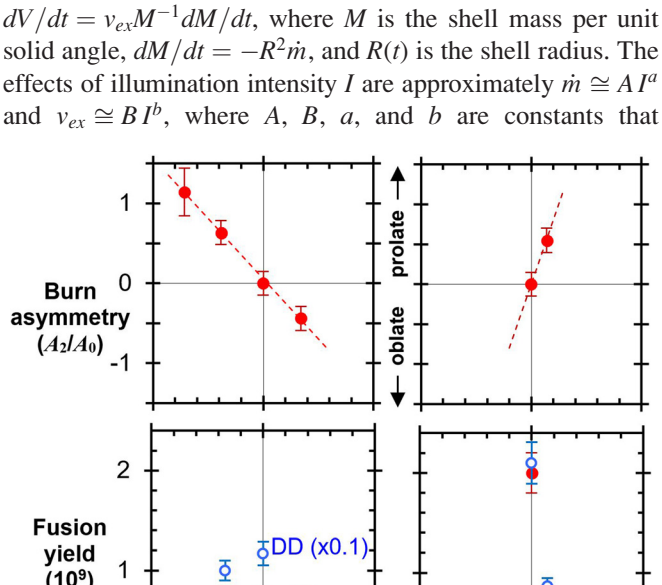

FIG. 6. Measured dependence of nuclear burn asymmetry (top plots) and fusion yield (bottom plots) on drive asymmetry for spherical capsules (left) and on shell-thickness asymmetry for spherical drive (right). The dashed lines indicate trends and are not quantitative fits or predicted extrapolations. All yields decrease quickly as the burn region loses spherical symmetry.

differ for direct and indirect drive.[1] If I is independent of time during the laser pulse, and if M_0 and M_1 are initial and final values of M, then the final V is $V_1 = v_{ex}\ln(M_0/M_1) = -v_{ex}\ln(1-f)$, where f is the fraction of the shell thickness ablated away. If M_0 (or I) is independent of angle θ on the shell, higher I (or lower M_0) on one shell segment than others leads to higher dV/dt. At the end of the acceleration phase, that segment has traveled farther and has a higher V; by the end of the coasting phase, the velocity differential leads to an even larger difference in R. Since most of the radial convergence has taken place by this time, any asymmetry in R going into the deceleration phase results in asymmetry in the assembled fuel and burn.

Treating each shell segment for the moment as independently described by the rocket equations, $M_0(\theta)$ can be chosen so V is independent of θ at the end of the acceleration phase for a given $I(\theta)$. In particular, if reference values M_{0r} and I_r are known to generate good performance, with resulting values f_r and V_r, then[24]

$$\frac{M_0(\theta)}{M_{0r}} \cong \left[\frac{I(\theta)}{I_r}\right]^a \left(\frac{1-e^{-V_r/BI_r^b}}{1-e^{-V_r/BI(\theta)^b}}\right) = \left[\frac{I(\theta)}{I_r}\right]^a \frac{f_r}{1-(1-f_r)^{\left[I(\theta)/I_r\right]^{-b}}} \quad (1)$$

or, for small deviations $dI(\theta)$ about $\langle I\rangle$,

$$\frac{dM_0(\theta)}{\langle M_0\rangle} \approx \left[a - b\frac{(1-\langle f\rangle)}{\langle f\rangle}\ln(1-\langle f\rangle)\right]\frac{dI(\theta)}{\langle I\rangle}. \quad (2)$$

Numerical integration of the rocket equations shows that this results in all shell segments having essentially the same V and the same R at the end of the acceleration phase, and therefore also at the end of the coasting phase, even if the laser pulse shape is not flat. This rough scaling should greatly reduce the fuel asymmetry that would otherwise occur due to $I(\theta)$ at burn-time. More accurate calculation of $M_0(\theta)$ requires full simulations that include effects of other processes such as the final deceleration of the shell, any possible lateral mass flow in the shell due to lateral pressure gradients, and shock waves; but Eq. (1) can be used to define a first trial distribution for $M_0(\theta)$.

Application of this scaling requires the constants $a = b = 1/3$ for direct drive, or $a = 3/4$ and $b = 1/8$ for indirect drive.[1] For the direct-drive experiments discussed here, f can be estimated by using the fact that a total laser power of 22 kJ in a 1-ns pulse at OMEGA ablates away ≈10–12 μm of a CH shell.[25] The mean shell thicknesses here were 17–20 μm, so $\langle f\rangle \approx 0.6$ and $dM_0(\theta)/\langle M_0\rangle \approx 0.5\ dI(\theta)/\langle I\rangle$. For P_2 asymmetries this is equivalent to $(A_2/A_0)_{\text{shell}} \approx 0.5\ (A_2/A_0)_{\text{drive}}$, which is very similar to the $(A_2/A_0)_{\text{shell}} \approx 0.4\ (A_2/A_0)_{\text{drive}}$ that was estimated above directly from data; that similarity inspires confidence that shimming according to a scaling such as that of Eqs. (1) or (2) should, at the very least, lead to significant reduction of implosion asymmetry when drive is asymmetric.

IV. CONCLUSION

In summary, we have made quantitative, 3D observations of the individual effects of low-mode drive

asymmetries and capsule shell asymmetries on nuclear burn symmetry and on fusion yield; compared the burn images favorably with x-ray images; and predicted quantitatively how target shimming might compensate for asymmetric drive.

The images do not show what happens before nuclear burn. In indirect drive, particularly, it is known that the symmetry of a capsule can sometimes "swing" during compression, introducing complications to implosion dynamics.[26] This results in a fraction of the total available energy being converted to nonradial motion, thus robbing the hot spot of some energy it would otherwise have. Nevertheless, the burn images show the configuration of the hot fuel at the time of compression burn, and thus illustrate the total net effect of all physical processes occurring as a direct-drive capsule implodes.

Definitive experiments involving both drive asymmetry and capsule shimming simultaneously have only recently been performed, in the context of polar-direct drive,[10] and an upcoming campaign at the NIF will explore capsule shimming in indirect drive.[11]

ACKNOWLEDGMENTS

We thank the OMEGA staff for their help in making these experiments possible. The work described here was supported in part by U.S. DOE Grants Nos. DE-NA0002726 and DE-NA0002949.

APPENDIX: SPATIAL RESOLUTION AND STATISTICAL NOISE IN THE BURN IMAGES

Reconstruction of burn images from raw penumbral data requires filtering to suppress statistical noise that results from the finite number of D^3He protons detected.[12] The filtering used here is adjusted so RMS image noise outside the burn region does not exceed about 10% of the peak emission level. The result is effectively a convolution of the true burn distribution with a two-dimensional Gaussian. That Gaussian has a FWHM of 20 μm for all burn images shown here except for those from the case $(A_2/A_0)_{\text{drive}} = -0.36$, where the very low proton yield required a value of 35 μm. The size of this Gaussian determines the image spatial resolution, and it also determines the size of the dominant image noise structure.[12]

This is useful information for calculating accurate sizes and asymmetries from any images that required a lot of filtering because of low proton yields, like those of Fig. 3(a). To determine absolute burn-region dimensions, we can model the source as an ellipsoid with Gaussian radial profiles (or two ellipsoids, in the case of Fig. 3(a)) and adjust radii so that, convolved with the appropriate filter, the result makes the best match to the image. The model can then be compared directly to x-ray images that have better spatial resolution, as shown in Fig. 4 for the burn image of Fig. 3(a).

[1]J. D. Lindl, *Inertial Confinement Fusion* (Springer-Verlag, New York, 1999).
[2]S. Atzeni and J. Meyer-ter-Vehn, *The Physics of Inertial Fusion* (Clarendon Oxford, 2004).
[3]T. R. Boehly, D. L. Brown, R. S. Craxton, R. L. Keck, J. P. Knauer, J. H. Kelly, T. J. Kessler, S. A. Kumpan, S. J. Bucks, S. A. Letzring, F. J. Marshall, R. L. McCrory, S. F. B. Morse, W. Seka, J. M. Soures, and C. P. Verdon, Opt. Commun. **133**, 495 (1997).
[4]P. Amendt, T. J. Murphy, and S. P. Hatchett, Phys. Plasmas **3**, 4166 (1996).
[5]L. J. Suter, A. A. Bauer, L. V. Powers, D. B. Ress, N. Delameter, W. W. Hsing, O. L. Landen, A. R. Thiessen, and R. E. Turner, Phys. Rev. Lett. **73**, 2328 (1994).
[6]P. Michel, S. H. Glenzer, L. Divol, D. K. Bradley, D. Callahan, S. Dixit, S. Glenn, D. Hinkel, R. K. Kirkwood, J. L. Kline, W. L. Kruer, G. A. Kyrala, S. Le Pape, N. B. Meezan, R. Town, K. Widmann, E. A. Williams, B. J. MacGowan, J. Lindl, and L. J. Suter, Phys. Plasmas **17**, 056305 (2010).
[7]S. Skupsky, J. A. Marozas, R. S. Craxton, R. Betti, T. J. B. Collins, J. A. Delettrez, V. N. Goncharov, P. W. McKenty, P. B. Radha, T. R. Boehly, J. P. Knauer, F. J. Marshall, D. R. Harding, J. D. Kilkenny, D. D. Meyerhofer, T. C. Sangster, and R. L. McCrory, Phys. Plasmas **11**, 2763 (2004).
[8]M. Hohenberger, P. B. Radha, J. F. Myatt, S. LePape, J. A. Marozas, F. J. Marshall, D. T. Michel, S. P. Regan, W. Seka, A. Shvydky, T. C. Sangster, J. W. Bates, R. Betti, T. R. Boehly, M. J. Bonino, D. T. Casey, T. J. B. Collins, R. S. Craxton, J. A. Delettrez, D. H. Edgell, R. Epstein, G. Fiksel, P. Fitzsimmons, J. A. Frenje, D. H. Froula, V. N. Goncharov, D. R. Harding, D. H. Kalantar, M. Karasik, T. J. Kessler, J. D. Kilkenny, J. P. Knauer, C. Kurz, M. Lafon, K. N. LaFortune, B. J. MacGowan, A. J. Mackinnon, A. G. MacPhee, R. L. McCrory, P. W. McKenty, J. F. Meeker, D. D. Meyerhofer, S. R. Nagel, A. Nikroo, S. Obenschain, R. D. Petrasso, J. E. Ralph, H. G. Rinderknecht, M. J. Rosenberg, A. J. Schmitt, R. J. Wallace, J. Weaver, C. Widmayer, S. Skupsky, A. A. Solodov, C. Stoeckl, B. Yaakobi, and J. D. Zuegel, Phys. Plasmas **22**, 056308 (2015).
[9]D. A. Callahan, D. S. Clark, A. E. Koniges, M. Tabak, G. R. Bennett, M. E. Cuneo, R. A. Vesey, and A. Nikroo, Nucl. Instrum. Methods Phys. Res., Sect. A **544**, 9 (2005).
[10]F. J. Marshall, P. B. Radha, M. J. Bonino, J. A. Delettrez, R. Epstein, V. Yu. Glebov, D. R. Harding, C. Stoeckl, J. A. Frenje, M. Gatu Johnson, F. H. Séguin, H. Sio, A. Zylstra, and E. Giraldez, Phys. Plasmas **23**, 012711 (2016).
[11]V. A. Smalyuk, private communication (2015).
[12]F. H. Séguin, J. L. DeCiantis, J. A. Frenje, S. Kurebayashi, C. K. Li, J. R. Rygg, C. Chen, V. Berube, B. E. Schwartz, R. D. Petrasso, V. A. Smalyuk, F. J. Marshall, J. P. Knauer, J. A. Delettrez, P. W. McKenty, D. D. Meyerhofer, S. Roberts, T. C. Sangster, K. Mikaelian, and H. S. Park, Rev. Sci. Instrum. **75**, 3520 (2004).
[13]J. DeCiantis, S. Kurebayashi, C. K. Li, J. R. Rygg, B. E. Schwartz, R. D. Petrasso, J. A. Delettrez, S. P. Regan, V. A. Smalyuk, J. P. Knauer, F. J. Marshall, D. D. Meyerhofer, S. Roberts, T. C. Sangster, C. Stoeckl, K. Mikaelian, H. S. Park, and H. F. Robey, Rev. Sci. Instrum. **77**, 043503 (2006).
[14]F. H. Séguin, J. L. DeCiantis, J. A. Frenje, C. K. Li, J. R. Rygg, C. D. Chen, R. D. Petrasso, J. A. Delettrez, S. P. Regan, V. A. Smalyuk, V. Yu. Glebov, J. P. Knauer, F. J. Marshall, D. D. Meyerhofer, S. Roberts, T. C. Sangster, C. Stoeckl, K. Mikaelian, H. S. Park, H. F. Robey, and R. E. Tipton, Phys. Plasmas **13**, 082704 (2006).
[15]D. Ress, R. A. Lerche, R. J. Ellis, S. M. Lane, and K. A. Nugent, Rev. Sci. Instrum. **59**, 1694 (1988).
[16]C. R. Christensen, D. C. Wilson, C. W. Barnes, G. P. Grim, G. L. Morgan, M. D. Wilke, F. J. Marshall, V. Yu. Glebov, and C. Stoeckl, Phys. Plasmas **11**, 2771 (2004).
[17]L. Disdier, A. Rouyer, I. Lantuéjoul, O. Landoas, J. L. Bourgade, T. C. Sangster, V. Yu. Glebov, and R. A. Lerche, Phys. Plasmas **13**, 056317 (2006).
[18]G. P. Grim, N. Guler, F. E. Merrill, G. L. Morgan, C. R. Danly, P. L. Volegov, C. H. Wilde, D. C. Wilson, D. S. Clark, D. E. Hinkel, O. S. Jones, K. S. Raman, N. Izumi, D. N. Fittinghoff, O. B. Drury, E. T. Alger, P. A. Arnold, R. C. Ashabranner, L. J. Atherton, M. A. Barrios, S. Batha, P. M. Bell, L. R. Benedetti, R. L. Berger, L. A. Bernstein, L. V. Berzins, R. Betti, S. D. Bhandarkar, R. M. Bionta, D. L. Bleuel, T. R. Boehly, E. J. Bond, M. W. Bowers, D. K. Bradley, G. K. Brunton, R. A. Buckles, S. C. Burkhart, R. F. Burr, J. A. Caggiano, D. A. Callahan, D. T. Casey, C. Castro, P. M. Celliers, C. J. Cerjan, G. A. Chandler, C. Choate, S. J. Cohen, G. W. Collins, G. W. Cooper, J. R. Cox, J. R. Cradick, P. S. Datte, E. L. Dewald, P. Di Nicola, J. M. Di Nicola, L. Divol, S. N. Dixit, R. Dylla-Spears, E. G. Dzenitis, M. J. Eckart, D. C. Eder, D. H. Edgell, M. J. Edwards, J. H. Eggert, R. B. Ehrlich, G. V. Erbert, J. Fair, D. R. Farley, B.

Felker, R. J. Fortner, J. A. Frenje, G. Frieders, S. Friedrich, M. Gatu-Johnson, C. R. Gibson, E. Giraldez, V. Y. Glebov, S. M. Glenn, S. H. Glenzer, G. Gururangan, S. W. Haan, K. D. Hahn, B. A. Hammel, A. V. Hamza, E. P. Hartouni, R. Hatarik, S. P. Hatchett, C. Haynam, M. R. Hermann, H. W. Herrmann, D. G. Hicks, J. P. Holder, D. M. Holunga, J. B. Horner, W. W. Hsing, H. Huang, M. C. Jackson, K. S. Jancaitis, D. H. Kalantar, R. L. Kauffman, M. I. Kauffman, S. F. Khan, J. D. Kilkenny, J. R. Kimbrough, R. Kirkwood, J. L. Kline, J. P. Knauer, K. M. Knittel, J. A. Koch, T. R. Kohut, B. J. Kozioziemski, K. Krauter, G. W. Krauter, A. L. Kritcher, J. Kroll, G. A. Kyrala, K. N. La Fortune, G. LaCaille, L. J. Lagin, T. A. Land, O. L. Landen, D. W. Larson, D. A. Latray, R. J. Leeper, T. L. Lewis, S. LePape, J. D. Lindl, R. R. Lowe-Webb, T. Ma, B. J. MacGowan, A. J. MacKinnon, A. G. MacPhee, R. M. Malone, T. N. Malsbury, E. Mapoles, C. D. Marshall, D. G. Mathisen, P. McKenty, J. M. McNaney, N. B. Meezan, P. Michel, J. L. Milovich, J. D. Moody, A. S. Moore, M. J. Moran, K. Moreno, E. I. Moses, D. H. Munro, B. R. Nathan, A. J. Nelson, A. Nikroo, R. E. Olson, C. Orth, A. E. Pak, E. S. Palma, T. G. Parham, P. K. Patel, R. W. Patterson, R. D. Petrasso, R. Prasad, J. E. Ralph, S. P. Regan, H. Rinderknecht, H. F. Robey, G. F. Ross, C. L. Ruiz, F. H. Séguin, J. D. Salmonson, T. C. Sangster, J. D. Sater, R. L. Saunders, M. B. Schneider, D. H. Schneider, M. J. Shaw, N. Simanovskaia, B. K. Spears, P. T. Springer, C. Stoeckl, W. Stoeffl, L. J. Suter, C. A. Thomas, R. Tommasini, R. P. Town, A. J. Traille, B. Van Wonterghem, R. J. Wallace, S. Weaver, S. V. Weber, P. J. Wegner, P. K. Whitman, K. Widmann, C. C. Widmayer, R. D. Wood, B. K. Young, R. A. Zacharias, and A. Zylstra, Phys. Plasmas **20**, 056320 (2013). The approach they describe has the very nice feature of providing separate information about the spatial distribution of burn in the hot, central fuel and the spatial distribution of neutron scattering in the cooler outer fuel and shell.

[19]J. R. Rygg, A. B. Zylstra, F. H. Séguin, S. LePape, B. Bachmann, R. S. Craxton, E. M. Garcia, Y. Z. Kong, M. Gatu-Johnson, S. F. Khan, B. J. Lahmann, P. W. McKenty, R. D. Petrasso, H. G. Rinderknecht, M. J. Rosenberg, D. B. Sayre, and H. W. Sio, Rev. Sci. Instrum. **86**, 116104 (2015).

[20]The algorithm described in Ref. 12 has since been simplified. The last term in Eq. (1) of that paper has been absorbed into the spatial convolution filter $F_{\mathrm{conv}}(\mathrm{r})$ of Eq. (5), and the weighting factor $C(\mathrm{r})$ of Eqs. (4) and (7) has been reduced to the form described in footnote 47 of Ref. 14.

[21]F. J. Marshall, J. A. Delettrez, R. Epstein, V. Yu. Glebov, D. R. Harding, P. W. McKenty, D. D. Meyerhofer, P. B. Radha, W. Seka, S. Skupsky, V. A. Smalyuk, J. M. Soures, C. Stoeckl, R. P. J. Town, B. Yaakobi, C. K. Li, F. H. Seguin, D. G. Hicks, and R. D. Petrasso, Phys. Plasmas **7**, 2108 (2000).

[22]V. A. Smalyuk, T. R. Boehly, L. S. Iwan, T. J. Kessler, J. P. Knauer, F. J. Marshall, D. D. Meyerhofer, C. Stoeckl, B. Yaakobi, and D. K. Bradley, Rev. Sci. Instrum. **72**, 635 (2001).

[23]M. A. Russotto and R. L. Kremens, Rev. Sci. Instrum. **61**, 3125 (1990).

[24]More rigorously, the left side of Eq. (1) should have the coefficient $\int R_r^2(t)dt/\int R^2(\theta,t)dt$, with integrals taken over the laser pulse. This ratio is ignored here because it is almost exactly 1.0; when the implosion velocities are equalized, the radial positions are also nearly equalized (as verified by numerical integrations).

[25]J. A. Delettrez, D. K. Bradley, and C. P. Verdon, Phys. Plasmas **1**, 2342 (1994).

[26]R. P. J. Town, D. K. Bradley, A. Kritcher, O. S. Jones, J. R. Rygg, R. Tommasini, M. Barrios, L. R. Benedetti, L. F. Berzak Hopkins, P. M. Celliers, T. Döppner, E. L. Dewald, D. C. Eder, J. E. Field, S. M. Glenn, 1 N. Izumi, S. W. Haan, S. F. Khan, J. L. Kline, G. A. Kyrala, T. Ma, J. L. Milovich, J. D. Moody, S. R. Nagel, A. Pak, J. L. Peterson, H. F. Robey, J. S. Ross, R. H. H. Scott, B. K. Spears, M. J. Edwards, J. D. Kilkenny, and O. L. Landen, Phys. Plasmas **21**, 056313 (2014).